Int. J. Electrochem. Sci., 10 **(2015)** 8210 - 8223

International Journal of
ELECTROCHEMICAL
SCIENCE
www.electrochemsci.org

Electrochemical Investigation on Crevice Corrosion of P110 Steel by Using One-Dimensional Array Electrode

Chengqiang Ren[1,2,*], *Jianbo Chen*[2], *Lidong Pu*[2], *Li Liu*[2], *Yong Pan*[2], *Junying Hu*[1], *Taihe Shi*[1]

[1] State Key Laboratory of Oil and Gas Reservoir Geology and Exploitation, Southwest Petroleum University, Chengdu, 610500, PR China
[2] School of Materials Science and Engineering, Southwest Petroleum University, Chengdu, 610500, PR China
[*]E-mail: chengqiangren@163.com

Received: 13 June 2015 / *Accepted:* 17 July 2015 / *Published:* 26 August 2015

In order to understand the corrosion damage to the inner contact surface of screw thread joint between tubing and coupling, artificial crevice was built by one-dimensional array electrode. Potentiodynamic polarization (PDP) technique, electrochemical impedance spectroscopy (EIS), scanning electrochemical microscopy (SECM) and scanning electron microscope (SEM) were adapted to measure the electrochemical behavior for each array electrode at different sites in the crevice. The obvious crevice corrosion was found for P110 oil tube steel in the CO_2 dissolved brine solution. The blockout effect inhibits carbonic species adsorbing to steel and produces low pH, which elevates corrosion in the neighboring region to the occluded area. A multi-staged model for the crevice corrosion was proposed.

Keywords: artificial crevice, array electrode, electrochemical impedance spectroscopy, scanning electrochemical microscopy, potentiodynamic polarization technique

1. INTRODUCTION

Metal materials during use, there is likely to be formed a crevice between metal-to-metal or metal-to-non-metallic. When the gap is sufficiently wide for liquid to penetrate into the crevice and sufficiently narrow for the liquid in the crevice to be stagnant, a serious localized corrosion concentrates in crevice occurs. As a result, this corrosion type is called crevice corrosion [1].

Once the crevice presents, the electrochemical difference between the outside and inside is easy to establishing for the metal, which is favor to the corrosion macro-cell. Almost all metallic materials have the tendency of crevice corrosion. However, the metal with the nature of passivation and with the

protective corrosion product is more susceptive. Crevice corrosion is an extremely complex form of localized corrosion due to its nature of being difficult to detect [2]. Once occurrence of crevice corrosion, the corrosion rate of metal rapidly increases and the structural integrity is seriously destroyed [3].

As well known, the lap joint is one of the most common places observed the crevice. The downhole tubing string in the oil and gas well is composed by couplings connected of decades or hundreds of oil tubes. If different materials are selected for the oil tube and coupling, the galvanic corrosion may exist at joint [4]. Though the same material is used, the joint may also suffer from corrosion, because the threaded connection of joint, internal thread and external thread, may construct a gap and induce crevice corrosion, which leads to higher probability of corrosion failure to the joint than the oil tube itself. In case the integrity of the joint is damaged, the gas and fluid escape into the annulus between casing and tubing string. It brings a series of security problems during oil and gas exploitation. Therefore, it is necessary to research the crevice corrosion of tube steel. It is a key issue to the wellbore integrity.

At present, many studies have been done to understand the mechanism of crevice corrosion for different kinds of metal materials in diverse environments. Various methods have been proposed to investigate the corrosion process, such as in situ measurement (electrode potential, pH and chloride concentration, etc.) in occluded area [5-8] and mathematical model to predict corrosion development [9-13]. However, there still remain limitations. The array electrode as a relatively novel test method was widely used in corrosion field in recent years [14-18]. The crevice corrosion of steel (UNS no.G10350) in carbon dioxide and oxygen environments with the presence of an artificial crevice through the array electrode was reported [15]. The corrosion of steel in an artificial crevice was monitored by application of the multichannel electrode method in the work of Atsushi et al [16]. The crevice is always considered one-dimensional in mathematical models [1], which is due to the successive development from crevice opening to bottom. On the basis of the view, the one-dimensional array electrode is suitably adapted to research the mechanism of crevice corrosion.

The understanding on crevice corrosion of joint of casing and tubing string in aggressive oil and gas field environments needs further efforts. Thus, this work aims to investigate the crevice corrosion mechanism of P110 carbon steel in brine solution dissolved with CO_2 by adapting one-dimensional array electrode. The experimental results were analyzed and discussed.

2. EXPERIMENTAL

2.1. Material and environment

P110 steel was used in experiments. Its chemical composition (wt.%) includes 0.26% C, 0.25% Si, 1.71% Mn, 0.02% Ni, 0.05% Cr, 0.01% Mo, 0.01% Ti and Fe balance.

The sample sized 5mm in diameter and 20mm in length was prepared. The surface of each specimen was polished successively with 200, 400, 800 and 1200 grit silicon carbide paper. Then it

was degreased by acetone, cleaned by deionized water, rinsed by alcohol and dried by blow drier immediately in order to obtain clean and smooth surface.

The experimental solution, 3.5% NaCl, was prepared by analytical grade sodium chloride and deionized water. Before immersion of sample, the solution was deoxygenated by N_2 bubble for 4h, and CO_2 was injected to dissolve in the solution and maintained saturation state during exposure. Experiments were operated at 50 ^oC in the airtight electrolytic cell.

2.2 Artificial crevice

Four steel samples were embedded in epoxy resin in line with the diagrammatic sketch shown in Fig.1.

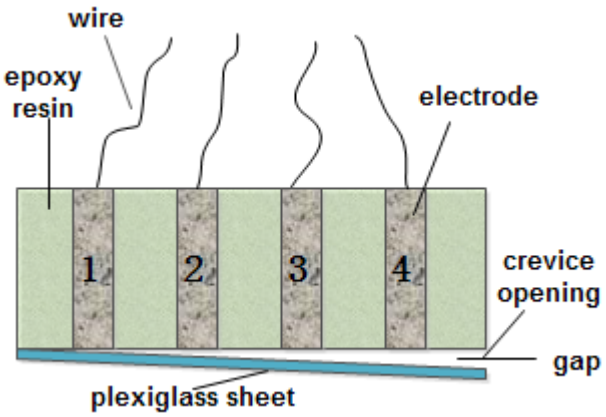

Figure 1. Schematic diagram of the artificial crevice

During this process, any crevice between steel sample and epoxy resin should be avoided. They were parallel arranged with an equal separated distance. This was the one-dimensional array electrode specimen. An artificial crevice was built by the surface of electrode specimen and transparent organic glass sheet. The crevice gap between the working electrode surface and organic glass sheet was adjusted to be 0.05, 0.1, 0.15 and 0.2 mm for each steel electrode from crevice bottom to opening respectively. The array electrodes were numbered $1^{\#}$, $2^{\#}$, $3^{\#}$ and $4^{\#}$ according to the order mentioned above. The array electrodes were coupled together by the copper wire when they immersed into the aggressive medium.

2.3 Electrochemical measurement

The Autolab Model PGSTAT302N electrochemical potentiostat was employed to perform EIS and PDP by using typical three electrode cell composed of working electrode (one-dimensional array electrode specimen), reference electrode (saturated calomel electrode) and auxiliary electrode (ring Pt). EIS measurements were operated under potentiostatic conditions at open circuit potential (E_{corr}) in a

frequency range from 100 KHz to 0.1 Hz, with an application of 5 mV amplitude sinusoidal voltage as disturbance signal when the corrosion time reached at 1h, 12h, 48h and 72h. PDP curves were obtained in a potential range from -400 mV to +400 mV versus E_{corr} with a scanning rate of 0.5 mV s^{-1}. All experiments were carried out when the electrochemical system was in steady state.

2.4 SECM test

The scanning electrochemical microscope equipment was consisted of a Model CHI900C tester and a 10 μm platinum probe, an Ag/AgCl/KCl (saturated) reference electrode and a platinum counter electrode. This technique, working in the amperometric mode, measured a faradaic current at the tip of probe at constant z across the sample surface (the x and y directions), while the tip was scanned over the sample after removal of corrosion product. Provided the current was controlled by diffusion of the electroactive species to the microelectrode. The currents measured were presented as current intensity at the probe. The measurements of line scans were generated with the tip at 10 μm from the specimen surface in all the cases. The scan rate was 80 μm/step.

2.5 SEM observe

The surface morphology of corrosion film after corrosion and the sample after removing corrosion product were observed by JSM-6490LV scanning electron microscope.

3. RESULTS AND DISCUSSION

3.1 Field statistics

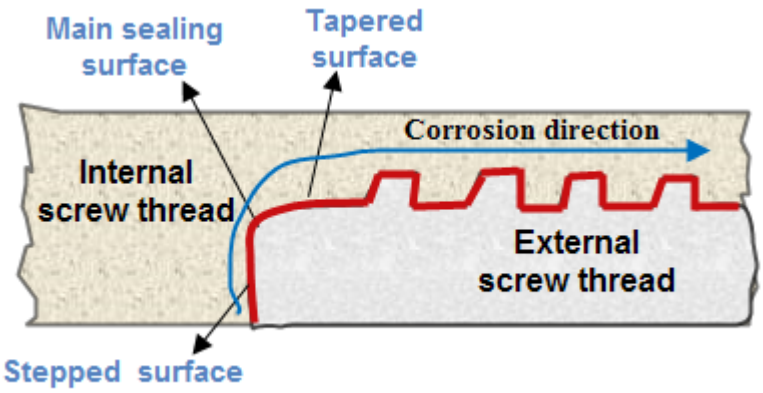

Figure 2. The structure and corrosion site of oilwell pipe column joint between tubing and coupling

Fig.2 shows the joint structure of oil tube and coupling and corrosion site from shoulder surface, main sealing surface and tapered surface to thread bite surface in the oilfield.

It was found more than 25% of tube strings were damaged by the corrosion failure of these areas among 250 investigated wellbore damaged wells. The most possibility for this corrosion is the

existence of the gap, which should be caused by either the mismatch between internal thread and external thread or the corrosion of inner surface of tube and coupling near the contact interface.

3.2 EIS plot

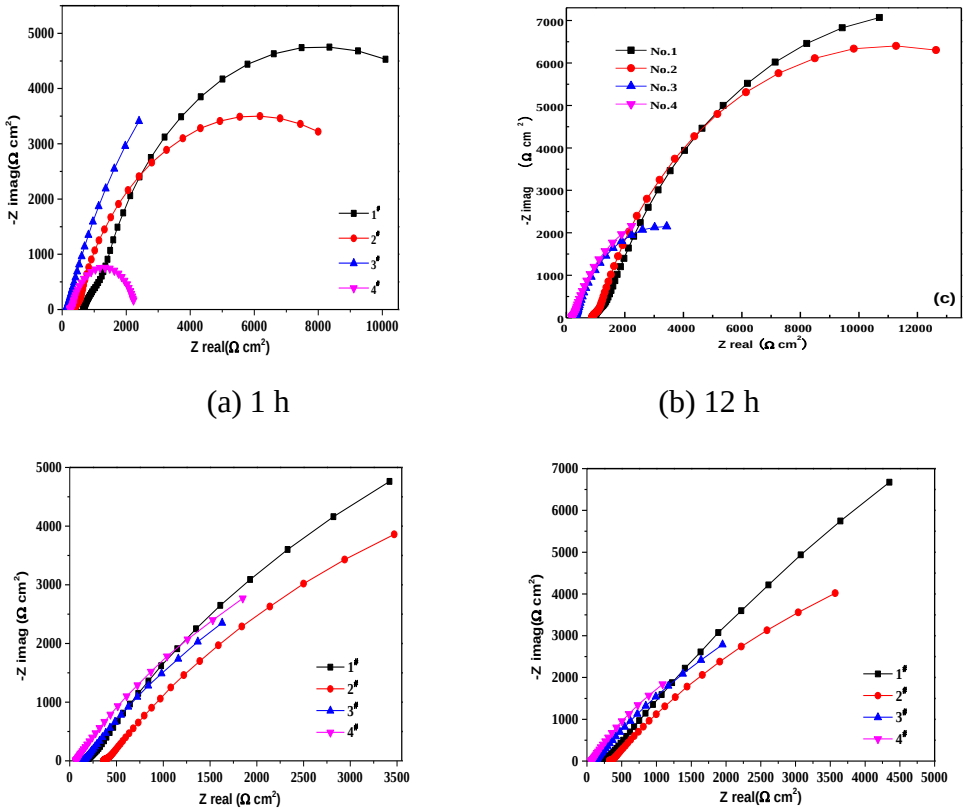

Figure 3. Nyquist plots for arrray electrode in CO_2 containing solution at different exposure times

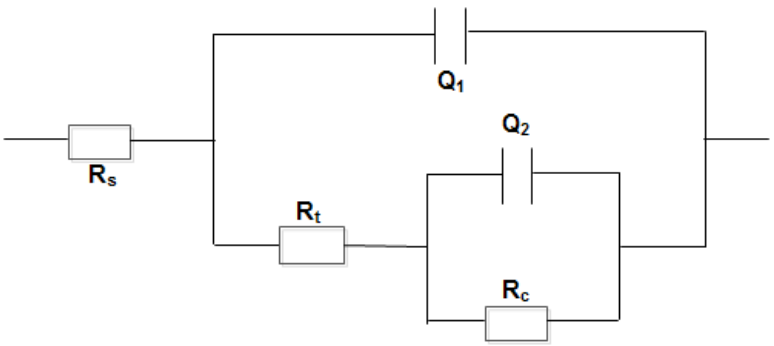

Figure 4. Equivalent circuit for array electrode to EIS

Fig.3 shows the Nyquist plots of the electrodes in NaCl solution dissolved with CO_2 at constant temperature of 50 ^{o}C.

All the plots were well fitted by the equivalent circuit with two time constants pictured in Fig. 4. Each Nyquist plot includes a high frequency capacitance loop (relatively small semi-circle) and a low frequency capacitance loop (relatively big semi-circle). Here, the high frequency capacitance loop reflects the electron transfer at the monitoring site, but the low frequency one is corresponding to the diffusion of aggressive substances or products [19, 20]. The parameters are the solution resistance (R_s), the charge-transfer resistance (R_t), the double layer capacitance (Q_{dl}), substance-transfer resistance (R_c) and capacitance (Q_c). Where, R_t is inverse ratio with corrosion reaction rate [21]. R_t values for each array electrode at different times were calculated by equivalent circuit fitting. The change tendencies are listed in Fig. 5.

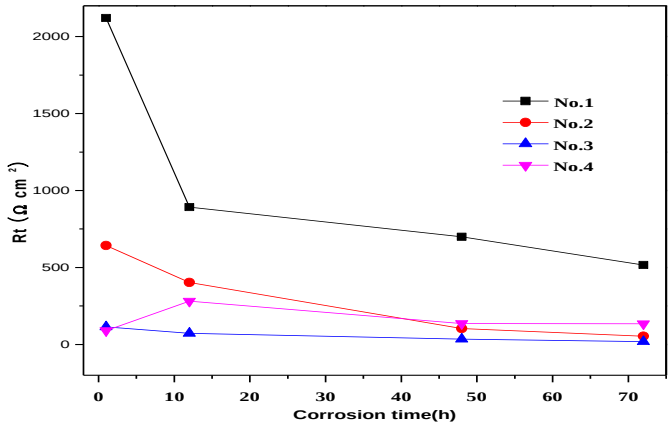

Figure 5. Variation of charge transfer resistance (R_t) with exposure time for array electrode

At 1 h, R_t values of 2010 Ω.cm^2, 643.1 Ω.cm^2, 114.2 Ω.cm^2, and 90.06 Ω.cm^2 for electrode 1$^{\#}$, 2$^{\#}$, 3$^{\#}$ and 4$^{\#}$are obtained. It's obviously deduced that the corrosion rate decreases with the declining opening dimension when the steel is bare. After 12 h immersion, only 4$^{\#}$ electrode presents elevated corrosion resistance, but the others descend. 3$^{\#}$ electrode shows higher reaction rate than 4$^{\#}$ electrode. It reveals that the incubation period for 3$^{\#}$ electrode is finished, namely, crevice corrosion comes into being. 4$^{\#}$ electrode is covered by corrosion product, and thus blockout effect is occurred. And further the corrosion rate of 2$^{\#}$ electrode is enhanced higher than 4$^{\#}$ electrode after 48 h immersion. This demonstrates that the crevice corrosion gradually moves forward the bottom of the crevice, which results from the continuous expanded gap size caused by corrosion. The crevice corrosion is not observed for 1$^{\#}$ electrode due to its higher R_t value than the outer electrodes even at 72 h. The smaller gap size has the longer incubation period of crevice corrosion. The value of charge transfer resistance of 3$^{\#}$ electrode is very low at 72h, which may reflect pitting on the electrode. Certainly, materials and corrosion environments are also play important role on the incubation period. Under our considered conditions, the crevice corrosion is easy to produce while the gap size meets the requirement.

3.3 Polarization curve

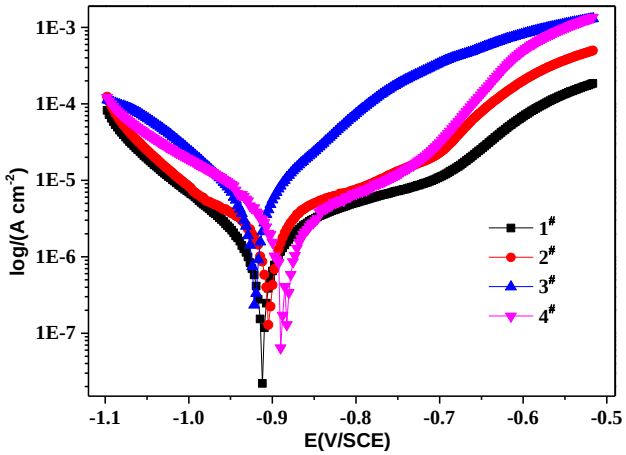

Figure 6. Polarization curve for array electrode after 72 h exposure

The polarization curves for array electrodes in carbon dioxide saturated brine solution after 72 h exposure are given in Fig.6. The corrosion rate is determined by the corrosion current density (i_{corr}), which can be obtained by extrapolation to the anodic and cathodic polarization curves. The controlling factor can be judged from polarization slopes (b_a and b_k):

$$b_a = \frac{2.3RT}{\alpha nF} \quad (1)$$

$$b_k = \frac{2.3RT}{(1-\alpha)nF} \quad (2)$$

Where α is the transfer coefficient for a given reaction, F is the Faraday constant (96490 C/equiv), R is the universal gas constant (8.314 J/(mol K)), and T is the absolute temperature (K). The calculated parameters are listed in Table 1.

Table 1. Tafel polarization data for array electrode calculated from polarization curves after 72 h exposure

Array electrode	Tafel data		
	I_{corr}(μA cm^{-2})	b_a(mVd^{-1})	b_k(mVd^{-1})
1#	2.73	270	105
2#	13.80	249	117
3#	20.50	104	110
4#	10.23	203	141

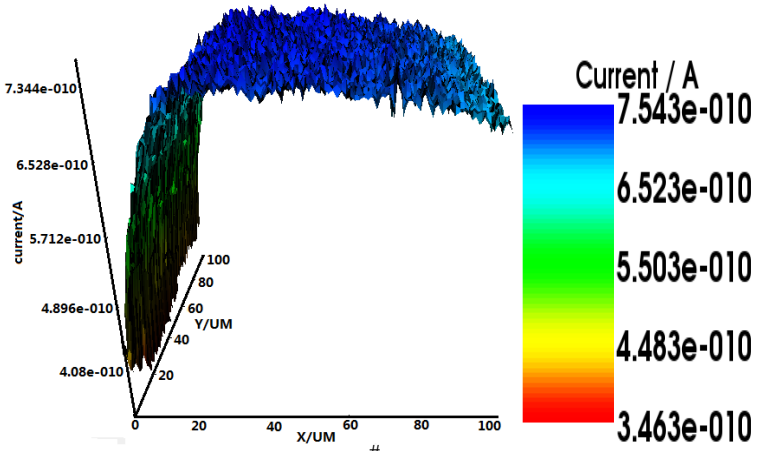

(a) 1# electrode

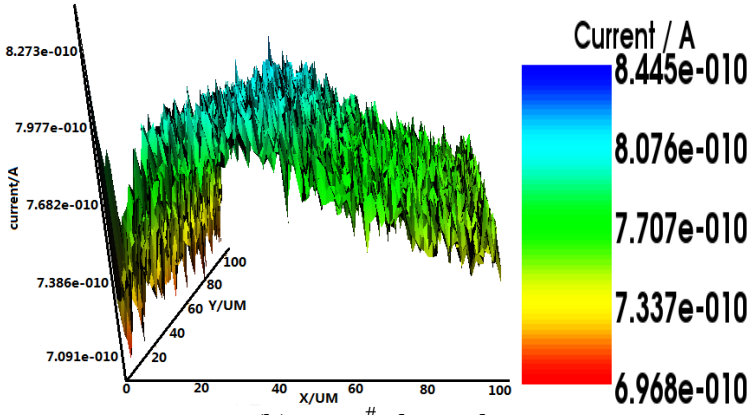

(b) 2# electrode

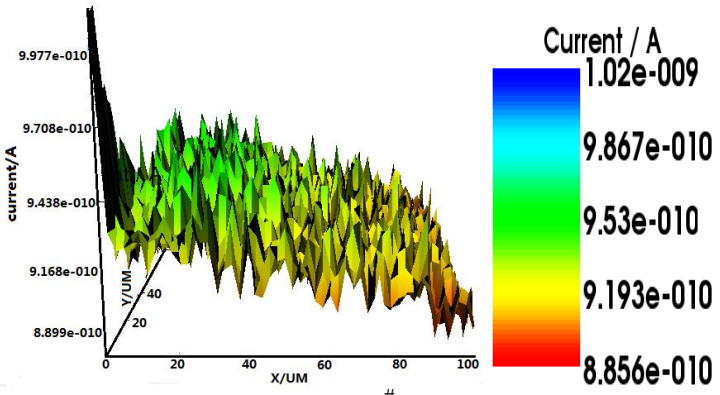

(c) 3# electrode

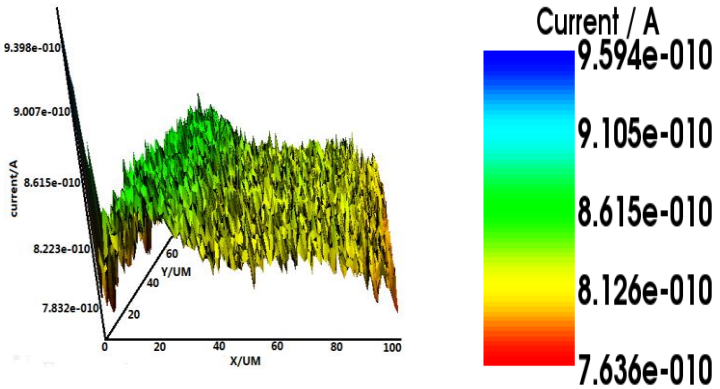

(c) 4# electrode

Figure 7. SECM images of different electrodes after removal of corrosion films

The order of i_{corr} follows $3^{\#}$ electrode > $2^{\#}$ electrode > $4^{\#}$ electrode > $1^{\#}$ electrode. $3^{\#}$ electrode endures the highest corrosion rate, which indicates the $4^{\#}$ electrode forms blockout effect to the inner electrodes, especially for $3^{\#}$ electrode. There is a superposition of diffusion polarization to the anodic current for $1^{\#}$ electrode, $2^{\#}$ electrode and $4^{\#}$ electrode in the range of 200 mV anodic polarization near corrosion potential, which inhibits the corrosion rate. Nesic [22] proposed an explanation to the anodic reaction in the solution at pH>5 presence of CO_2:

$$Fe + CO_2 \Leftrightarrow Fe_L \quad (3)$$

$$Fe_L + H_2O \Leftrightarrow Fe_LOH_{ad} + H^+ + e^- \quad (4)$$

$$Fe_LOH_{ad} \xrightarrow{rds} Fe_LOH^+_{ad} + e^- \quad (5)$$

$$Fe_LOH^+_{ad} + H_2O \Leftrightarrow Fe_L(OH)_{2ad} + H^+ \quad (6)$$

$$Fe_L(OH)_{2ad} \Leftrightarrow Fe_L(OH)_{2sol} \quad (7)$$

$$Fe_L(OH)_{2sol} + 2H^+ \Leftrightarrow Fe^{2+} + CO_2 + 2H_2O \quad (8)$$

Where the ligand Fe_L = Fe–CO_2 is formed as an adsorbed species at the electrode surface. The subscript *ad* and *sol* represent adsorption state and solution-state respectively. Thus, at the opening and the bottom of crevice, the pH is high, so adsorption of carbonic species to iron is necessary. For $4^{\#}$ electrode, corrosion film hinders the carbonic species contacting the steel. When the blockout effect becomes markedly, corrosion is accelerated for $3^{\#}$ electrode due to the diffusion and enrichment of Cl^- from bulk solution out of the crevice. The acidity is promoted caused by the hydrolysis of $FeCl_2$.

$$FeCl_2 + 2H_2O \Leftrightarrow Fe(OH)_2 + 2HCl \quad (9)$$

The anodic reaction mechanism may transfer to other processes when pH<5, for example, the mechanism suggested by Bockris et al. [23] in stronger acid attributed by the adsorption of H_2O:

$$Fe + H_2O \Leftrightarrow FeOH + H^+ + e^- \quad (10)$$

$$FeOH \xrightarrow{rds} FeOH^+ + e^- \quad (11)$$

$$FeOH^+ + H^+ \Leftrightarrow Fe^{2+} + H_2O \quad (12)$$

Therefore, pure electrochemical polarization is found for $3^{\#}$ electrode, and the anodic polarization degree is weakened. Meanwhile, H^+ is the cathodic depolarizer in CO_2 dissolved solution in nature, so the cathodic reaction rate is also elevated. Based on the acceleration to both anodic and cathodic reaction, the corrosion rate of $3^{\#}$ electrode is necessarily the highest one. $1^{\#}$ electrode and $2^{\#}$ electrode, nevertheless, still abide by the Nesic model due to the high pH, because the accumulation of Cl^- is not enough at this time.

3.4 SECM difference

SECM is one kind of chemical microscope with high spatial resolution which can directly characterize the surface morphology of substrate electrode and electrochemical activity distribution through the changes of Faraday current distribution measured by scanning microprobe [24,25]. Therefore, scanning electrochemical microscopy has been widely applied in corrosion research to reflect not only the diffusion of mediator but also the separation distance [26-29].

The status of a corroded sample was studied by monitoring the probe (tip potential: 0.5 V vs Ag/AgCl/saturated KCl reference electrode) and the substrate (tip potential: -0.7 V) in the solution.

The three-dimensional images of probe current in 100×100 μm^2 square surface are displayed in Fig. 7. It is clear, by comparing different locations in the crevice, that the redox current in local regions on electrode surface has large difference. On the one hand, the top currents of $2^{\#}$ electrode, $3^{\#}$ electrode and $4^{\#}$ electrode are higher than $1^{\#}$ electrode, which has a relationship to the regeneration of redox mediator in the specimen surface. It should be attributed to the increase of ionic strength within the gap between the steel surface and the Pt probe due to dissolved Fe^{2+} ions and/or the removal of the surface film from the steel thus exposing the underlying metal. The decrease in current also reflects the elevating insulating surface [30], which is caused by the corrosion product. This result supports the corrosion tendency by electrochemical data including EIS and polarization curve discussed in the front exposition. On the other hand, the most stable current distribution is observed for $1^{\#}$ electrode. $3^{\#}$ electrode, however, presents the greatest fluctuation. Current variation in each sample is more possible to the separation distance. Therefore, $3^{\#}$ electrode inevitably suffers from localized corrosion. In brief, at the bottom of the crevice ($1^{\#}$ electrode), the size is not enough initiating crevice corrosion, and the localized corrosion accelerates damage to the corrosion sensitive place.

3.5 Surface feature

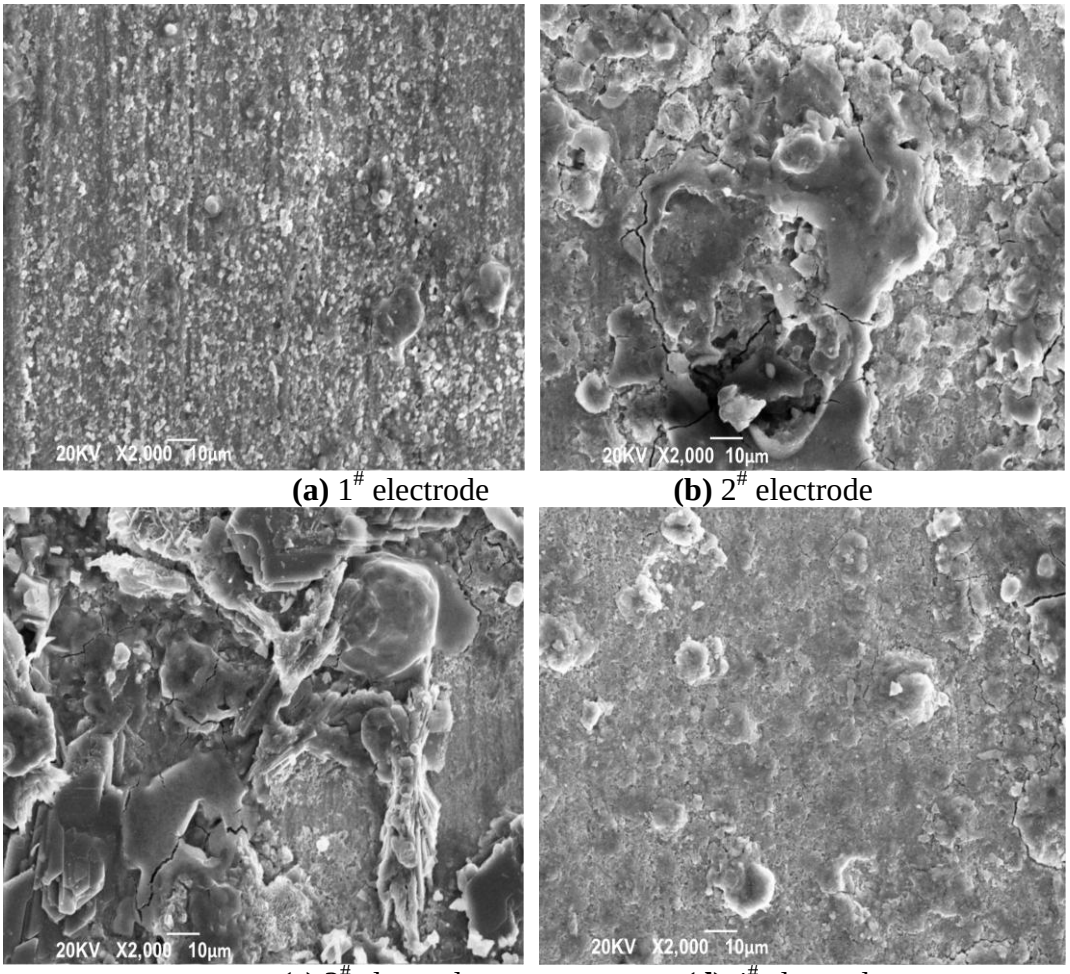

(a) $1^{\#}$ electrode **(b)** $2^{\#}$ electrode

(c) $3^{\#}$ electrode **(d)** $4^{\#}$ electrode

Figure 8. SEM micrographs of corrosion product layer on different electrode surfaces

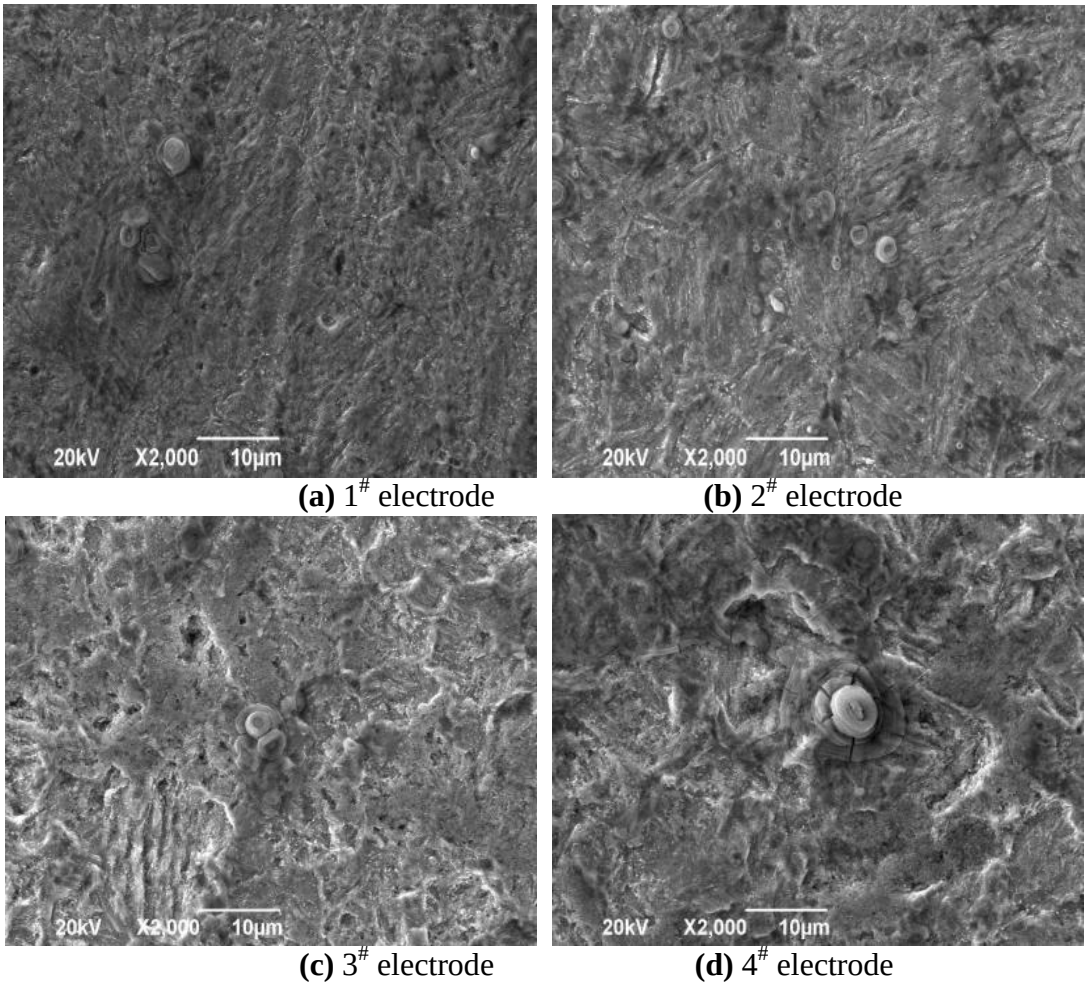

(a) $1^{\#}$ electrode **(b)** $2^{\#}$ electrode

(c) $3^{\#}$ electrode **(d)** $4^{\#}$ electrode

Figure 9. SEM micrographs of different electrode surfaces after removing the corrosion product layer

SEM photographs were taken to show the corrosion degree of array electrodes after 72 h exposure. Fig. 8 shows the corrosion film on the surface of each electrode. The microstructure observed for $2^{\#}$ electrode is similar to $3^{\#}$ electrode. The corrosion products accumulate disorderly and present loose and detached feature. However, denser corrosion film is found for $4^{\#}$ electrode, which is favor of blackout effect, and slight corrosion can be judged from the thin film on the surface of $1^{\#}$ electrode. Also the surface morphology after removing the corrosion product layer is shown in Fig. 9. It is notable that pitting initiates on $3^{\#}$ electrode from nanometers to micrometers, which is corresponding to lowest value of R_t and leads to propagation of crevice corrosion while size grows enough. When the crevice sizes of $3^{\#}$ electrode and $2^{\#}$ electrode expand by corrosion, $3^{\#}$ electrode and $2^{\#}$ electrode gradually replace the role of $4^{\#}$ electrode and $3^{\#}$ electrode. This process continuous develops from outer to the inner in crevice during long time exposure. As a result, the damage to the whole contact face is not at all surprising.

3.6 Crevice corrosion model

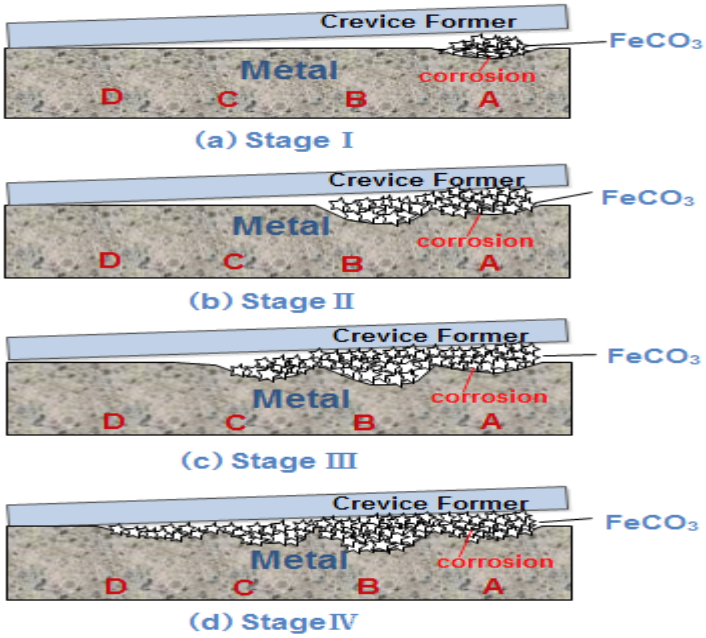

Figure 10. Multi-staged crevice corrosion model for P110 steel in NaCl solution containing CO_2

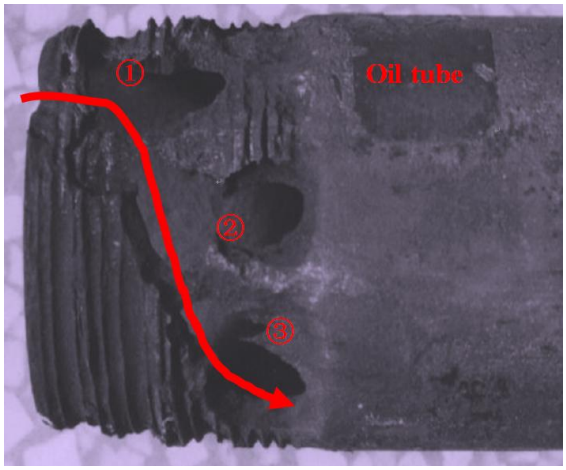

Figure 11. Corrosion feature of tubing at screw thread from field investigation

On the basis of the results and discussions clarified above, the crevice corrosion model is proposed in Fig. 10. At the first stage, the outer part in the crevice is primary corrosion. When the size is suitable, the products, $FeCO_3$, should block up the opening of the crevice (labeled as A). The next process is the more serious corrosion in region B which is near A, including incubation and propagation periods. It is different to the crevice corrosion in brine solution with O_2 which mainly determined by cathodic reaction for oxygen concentration cell [31]. In the CO_2 dissolved solution, anodic and cathodic polarizations are both weakened. The concentration cell is no longer the dominant factor to the crevice corrosion. Cl^- is still a well known catalytic agent for the crevice corrosion [32].

The front of B region extends inward, and the inner part of crevice also occurs corrosion with a lower rate, so the two aspects make the size of C region is enough to initiating crevice corrosion after a certain exposure time. This continuously develops toward the bottom of the crevice till the damage to the whole joint. Fig. 11 displays the corrosion failure picture of screw thread of tube downhole the well. The corrosion originates from the edge of screw thread and pushes ahead gradually liking the direction of arrow, which at least endures three durations. It presents typical feature of multi-staged propagation of crevice corrosion.

4. CONCLUSIONS

Corrosion damage to inner contact surface of screw thread joint between tubing and coupling is a common case in the oil and gas wells. Therefore, four parallel arranged electrodes in the artificial crevice were synchronously measured during exposure.

(1) The obvious crevice corrosion is found for P110 steel in CO_2 containing brine solution. The most incidental gap size is between 0.1 to 0.15 mm.

(2) The crevice corrosion is accompanied by pitting, which provides strong damage to the screwed connection.

(3) Based on the field and lab investigations, a multi-staged model for the crevice corrosion of tubing joint was proposed. It can well explain the development of the crevice corrosion.

ACKNOWLEDGEMENT
The authors thank financial supports by National Natural Science Foundation of China (51374180), open fund (PLN1306) of State Key Laboratory of Oil and Gas Reservoir Geology and Exploitation (Southwest Petroleum University) and Key Lab of Material of Oil and Gas Field (X151515KCL08)

References

1. E. Bardal, Corrosion and Protection, *Springer*, 2004:108.
2. M. I. Abdulsalam, H. W. Pickering, *Corros .Sci*. 41(1998)351.
3. A. Naganuma, K. Fushimi, K. Azumi, H. Habazaki and H. Konno, *Corros .Sci*. 52(2010)1179.
4. C. Ren, M. Zhu, L. Du, J. Chen, D. Zeng, J. Hu and T. Shi, *Int. J. Electrochem. Sci*.10(2015)4029.
5. A. Naganuma, K. Azumi, *Corros. Sci*. 53(2011)1165.
6. R. C. Wolfe, K. G. Weil and H. W. Pickering, *J. Phys. Chem.* B. 108 (2004) 14298.
7. H. Wang, J. Wang, C. Fu and K. Wang, *Int. J. Electrochem. Sci*. 8 (2013) 8812.
8. E. Otero, J. A. González, B. Chico and M. Morcillo, *Mater. Corros*. 53 (2002) 807.
9. G. F. Kennell, R. W. Evitts and K. L. Heppner, *Corros . Sci*. 50 (2008) 1716.
10. F. M. Song, *Electrochim. Acta*. 56 (2011) 6789.
11. W. Sun, L. Wang, T. Wu and G. Liu, *Corros. Sci*. 78 (2014) 233.
12. Z. Wang, Y. Cong, T. Zhang, Y. Shao and G. Meng, *Int. J. Electrochem. Sci*, 6 (2011) 5521.
13. K. L. Heppner, R. W. Evitts and J. Postlethwaite, *Can. J. Chem. Eng*. 80 (2002) 849.
14. Y. Wang, W. Wang, Y. Liu, L. Zhong and J. Wang, *Corros. Sci*. 53 (2011) 2963.
15. Y. J. Tan, S. Bailey and B. Kinsella, *Corros. Sci*. 43 (2001) 1919.

16. A. Naganuma, K. Fushimi, K. Azumi, H. Habazaki and H. Konno, *Corros. Sci*. 52 (2010) 1179.
17. Y. Tan, *Corros*. 54 (1998) 403.
18. Y. J. Tan, S. Bailey, B. Kinsella and A. Lowe, *J. Electrochem Soc*. 147 (2000) 530.
19. A. Bautista, A. González-Centeno, G. Blanco and S. Guzmán, *Mater. Charact.* 59 (2008) 32.
20. S. L. Wu, Z. D. Cui, G. X. Zhao, M. L. Yan, S. L. Zhu and X. J. Yang, *Appl. Surf. Sci*. 228 (2004) 17.
21. Y. Chen, W. P. Jepson, *Electrochim. Acta.* 44 (1999) 4453.
22. S. Nesic, *Corros. Sci.* 49 (2007) 4308.
23. J. M. Bockris, D. Drazic and A. R. Despic, *Electrochim. Acta.* 4 (1961) 325.
24. S. Rhode, V. Kain, V. S. Raja and G. J. Abraham, *Mater. Charact.* 77 (2013) 109.
25. M. A. Edwards, S. Martin, A. L. Whitworth, J. V. Macpherson and P. R. Unwin, *Physiol Meas.* 27 (2006) R63.
26. G. Wittstock , M. Burchardt, S. E. Pust, Y. Shen and C. Zhao, *Angew. Chem. Int. Ed.* 46 (2007) 1584.
27. P. Sun, F. O. Laforge and M. V. Mirkin, *Phys. Chem. Chem. Phys.* 9 (2007) 802.
28. A. G. Marques, J. Izquierdo, R. M. Souto and A. M. Simões, *Electrochim. Acta.* 153 (2015) 238.
29. L. C. Abodi, Y. Gonzalez-Garcia, O. Dolgikh, C. Dan, D. Deconinck, J. M. C. Mol, H. Terryn and J. Deconinck, *Electrochim. Acta.* 146 (2014) 556.
30. A. Singh, Y. Lin, W. Liu, E. E. Ebenso and J. Pan, *Int. J. Electrochem. Sci*. 8 (2013)12884.
31. F. M. Song and N. Sridhar, *Corros. Sci*. 50 (2008) 70.
32. Y. Z. Yang, Y. M. Jiang and J. Li, *Corros. Sci*. 76 (2013) 163.